ELSEVIER

Chemical Engineering Journal 137 (2008) 30–37

Chemical Engineering Journal

www.elsevier.com/locate/cej

Studies on MCM-41 mesoporous silica for drug delivery: Effect of particle morphology and amine functionalization

M. Manzano [a], V. Aina [a], C.O. Areán [b], F. Balas [a], V. Cauda [a], M. Colilla [a], M.R. Delgado [b], M. Vallet-Regí [a,*]

[a] *Departamento de Química Inorgánica y Bioinorgánica, Facultad de Farmacia, Universidad Complutense de Madrid, 28040 Madrid, Spain*

[b] *Departamento de Química, Universidad de las Islas Baleares, 07122 Palma de Mallorca, Spain*

Received 28 May 2007; received in revised form 10 July 2007; accepted 12 July 2007

Abstract

Mesoporous MCM-41 silica functionalized by 3-aminopropyltriethoxysilane grafting was studied as a potential carrier for controlled drug release, using ibuprofen as a test drug. For comparison, non-functionalized MCM-41 was also investigated. For the purpose of testing the effect of carrier morphology on drug delivery rate, MCM-41 was prepared in the form of both, a powder consisting of irregularly shaped (and sized) particles and monodispersed spheres (490 to 770 nm in diameter). Amine-functionalized MCM-41 micro-spheres were found to show a significantly slower drug release rate than irregularly shaped powders, which should facilitate drug delivery control over a longer time period.

Keywords: Silica-based mesoporous materials; Drug delivery systems

1. Introduction

Controlled drug release aims at optimizing drug efficiency while simultaneously reducing adverse collateral effects. Several studies [1–3] have shown that pharmacokinetics, drug efficiency and suppression of undesired side effects in different pathological conditions (*e.g.* hypertension and rheumatoid arthritis) can be improved by correct timing of drug administration and controlled kinetics of drug release. To this end, porous drug carriers have been pharmaceutically exploited for a long time; among them, porous silica, polypropylene foams and porous magnesium aluminosilicate, which go under the trade names of Sylysia, Accurel and Neusilin, respectively. Porous texture is known to be an important factor controlling diffusion and, hence, drug delivery rate [4–9]. However, less studied factors are particle size and shape (morphology) and functionalization of the drug carrier. Morphology determines the extension of the interface between the drug-carrying particle and body fluids, and could thereby affect drug release kinetics [6,10]. Appropriate functionalization of the inner pore walls of the carrier would also potentially affect release rate by determining drug binding strength [6,11].

Aiming at a combined analysis of the effect of carrier morphology and functionalization, we report on a detailed study of ibuprofen uptake and release by MCM-41 type mesoporous silica prepared both, as an irregularly shaped powder and also in the form of microsized spheres. In both cases, pure MCM-41 and amine-functionalized samples were studied. MCM-41 was chosen on account of the following: (i) Silica shows high tolerance *in vivo*, and in fact it is currently being used in some pharmaceutical formulations [12]; (ii) MCM-41 can be synthesized as a highly ordered mesoporous material having a pore size ranging from about 2 to 8 nm; the pore system being unidimensional and highly regular for each particular preparation [13]; (iii) synthesis of microsized and monodispersed MCM-41 silica spheres is relatively easy to accomplish [14,15]; and (iv) MCM-41 type silica has been proposed as a convenient material for both drug [16–19] and gene [18,20] delivery. Ibuprofen was chosen as a test drug for two main reasons. First, ibuprofen is currently used in a range of pharmaceutical formulations as an analgesic and also as an anti-inflammatory drug (*e.g.* for medical treatment of rheumatoid arthritis). Second, cross-reference to recent studies on ibuprofen delivery by carriers based on both, mesoporous silica [4,21,22] and metal-organic framework systems [23], should

* Corresponding author. Tel.: +34 91 394 1843; fax: +34 91 394 1786.
E-mail address: vallet@farm.ucm.es (M. Vallet-Regí).

1385-8947/$ – see front matter © 2007 Elsevier B.V. All rights reserved.
doi:10.1016/j.cej.2007.07.078

facilitate extension of current knowledge in this field by giving a broader view.

2. Experimental

2.1. Synthesis of MCM-41 samples

Mesoporous MCM-41 silica having an irregular particle shape was synthesised by a self-assembly process of silica and surfactant in which inorganic and organic species (surfactant) simultaneously condense, giving rise to mesoscopically ordered composite formation [24,25]. The synthesis procedure was as follows. 5.139 g of hexadecyltrimethyl ammonium bromide (C_{16}TAB, 99%, Aldrich) was dissolved in 46.4 mL of water. Separately, 25 mL of tetraethyl orthosilicate (TEOS, 98%, Aldrich) was hydrolyzed in 11.8 mL of tetramethyl ammonium hydroxide (TMAOH, 25%wt. solution in water, Aldrich) and this solution was added to the former one, followed by further dropwise addition of 22.5 mL TEOS; the mixture was kept under continuous stirring until hydrolysis was complete. The obtained gel, which had the nominal composition 1TEOS:0.12C_{16}TAB:0.28TMAOH:26.2H_2O, was poured into a hermetically closed Teflon vessel and heated at 100 °C for 24 h. The resulting gel was then filtered, washed with distilled water and dried at 60 °C. In order to remove the surfactant, the powder was then heated at 550 °C, first under a nitrogen flow for 3 h and then in air for 3 h. Complete removal of the surfactant was checked by means of infrared spectroscopy and thermogravimetry, which did not reveal presence of any residual organic species. The MCM-41 sample thus obtained had an irregular particle size and shape (see Section 3) and will be hereafter termed **Irr**.

Three different samples consisting of mesoporous silica spheres having average particle diameter of *ca.* 490 nm (hereafter **Sph$_{490}$**), 615 nm (**Sph$_{615}$**), and 770 nm (**Sph$_{770}$**), respectively, were synthesized according to the procedure described by Liu et al. [14], which follows a variation [26] of Stöber's method [27]. C_{16}TAB was dissolved in a solution of aqueous ammonia and ethanol. After stirring for 15 min, TEOS was dropwise added and the mixture was kept under stirring for 2 h at room temperature for samples **Sph$_{615}$** and **Sph$_{770}$**, and at 75 °C for sample **Sph$_{490}$**. The nominal composition of the synthesis gel was 1TEOS:0.3C_{16}TAB:11NH_3:58EtOH:144H_2O for samples **Sph$_{490}$** and **Sph$_{615}$**; and 2TEOS:0.3C_{16}TAB:11NH_3:58EtOH:144H_2O for sample **Sph$_{770}$**. Note that gel composition and preparation temperature are known to be key parameters controlling size of the resultant silica spheres [26–28]. In each case, the solid product obtained was filtered, thoroughly washed with distilled water and ethanol and air-dried in a desiccator. Finally, in order to remove the C_{16}TAB surfactant and ammonia, the product was heated at 550 °C first in a nitrogen flow for 3 h and then in air for 3 more h.

2.2. Functionalization of MCM-41 samples

Amine-functionalized MCM-41 samples were prepared by treating them with 3-aminopropyltriethoxysilane (APTES, 99%, Fluka) as follows. Template-free MCM-41 materials were dehydrated at 70 °C for 4 h under a nitrogen flow and then refluxed with 5 mmol of APTES/g SiO_2 in toluene (99.5%, Aldrich) (10 mL of toluene per g of SiO_2) for 16 h at 120 °C. The obtained products were filtered, washed with a mixture of diethyl ether and dichloromethane (1:1) and finally dried at 60 °C for 12 h in air.

2.3. Materials characterisation

Several instrumental techniques were used for sample characterisation. Thermogravimetric (TG) and differential thermal analyses (DTA) were carried out between 30 and 950 °C at a heating rate of 10 °C/min (under a gentle air flow) using a Perkin-Elmer Pyris Diamond TG/DTA analyzer. Elemental analyses were performed on a Macroanalyzer Leco CNS-2000-I. Fourier transform infrared spectroscopy (FTIR) was performed on a Nicolet Nexus spectrometer using the KBr pellet method. Small angle XRD patters were recorded on a Philips X'Pert multi purpose diffractometer with a thin film attachment for low angle glazing incidence measurements. For this purpose, a parallel plate collimator was attached in the diffracted beam. The diffractometer was equipped with CuKα radiation (λ = 1.5406 Å) operating at 40kV and 20mA. The diffractograms were recorded over the range 0.6–10.0° (2θ) with a step size of 0.02° and an accumulation time of 5 s. Surface area and porosity were determined from nitrogen adsorption–desorption isotherms obtained (at −196 °C) on a Micromeritics ASAP2010 analyzer. In all cases, 50–70 mg of material was degassed at 60 °C for 24 h under a vacuum (residual pressure $<10^{-5}$ Torr) before nitrogen adsorption. Particle morphology was analyzed by scanning electron microscopy (SEM) using a Hitachi S-350 JSM 6335F field emission microscope operated at 12 kV. Solid-state ^{29}Si cross-polarised (CP) NMR spectra were recorded at room temperature on a Varian VXR-400S-WB spectrometer operated at 79.5 MHz, with a pulse width of 4 μs and a recycle delay of 60 s. Tetra-coordinated silicon centres were named with the conventional Q^n notation where Q stands for the $(SiO)_nSi(OR)_{4-n}$ unit and n is the number of bridging oxygen atoms surrounding the central silicon atom. Tri-coordinated silicon centres were denoted with the conventional T^n notation where T stands for $(SiO)_nR'Si(OR)_{3-n}$ and n is the number of bridging oxygen atoms surrounding the central silicon atom.

2.4. Ibuprofen loading and release measurements

Hexane is frequently used as a solvent for ibuprofen [4,6,16,22,29–31]. However, because of health concerns [32,33] pentane was chosen; ibuprofen is readily soluble in pentane and this solvent is essentially harmless for laboratory use. Powdered MCM-41 samples were loaded with ibuprofen (Normon laboratories SA) by soaking them, under continuous magnetic stirring for 24 h at 37 °C, into a pentane solution of ibuprofen (33 mg/mL). A 1:1 (by weight) ratio of ibuprofen to solid sample was used. Powder ibuprofen loaded samples were recovered by filtration, washed with pentane and left to dry for 24 h at 37 °C. Portions of 100 mg of ibuprofen loaded samples were then com-

pacted under uniaxial pressure (0.5 MPa) to obtain disk pieces having 13 mm diameter. Thermogravimetric and elemental analyses were performed to evaluate the percentage of ibuprofen adsorbed in each sample.

The *in vitro* drug delivery assays were performed by soaking the sample disks into a simulated body fluid, SBF [34], at 37 °C and at physiological pH of 7.4, maintaining the ratio SBF volume (mL) per adsorbed ibuprofen mass (mg) equal to 1. Continuous magnetic stirring was maintained during the delivery assays to avoid limitation of the delivery rate by external diffusion constrains. The delivered ibuprofen concentration was monitored by UV spectrometry at 273 nm using a UV-500 UNICAM spectrometer.

3. Results and discussion

3.1. Characterisation of MCM-41 materials

SEM images, depicted in Fig. 1, show that samples **Sph$_{490}$**, **Sph$_{615}$** and **Sph$_{770}$**, consist of microsized spheres; their corresponding diameter distribution was found to be very narrow and centred at 490, 615 and 770 nm, respectively. Statistical analysis on SEM micrographs (300 counted spheres for each sample) showed that 95% of the micro-spheres were within the following size distribution limits: **Sph$_{490}$**, 490 ± 60 nm; **Sph$_{615}$**, 615 ± 65 nm; **Sph$_{770}$**, 770 ± 60 nm. Sample **Irr**, on the other hand, consists of irregularly shaped particles, which have a very broad distribution of particle size going from less than 300 nm to more than 10 μm.

Table 1
Lattice parameter, a_0, and textural data for irregular and spherically shaped MCM-41 samples

Sample	a_0 (nm)	D_P (nm) KJS	V_P (cm3/g)	S_{BET} (m^2/g)
Irr	4.40	3.7	0.80	928
Sph$_{490}$	4.16	3.2	0.46	874
Sph$_{615}$	4.11	3.1	0.48	1078
Sph$_{770}$	4.21	3.6	0.58	1198

D_P: pore diameter obtained following the KJS method, V_P: pore volume, S_{BET}: surface area. The lattice parameter was calculated, from the corresponding $d_{(10)}$ spacing, as $a_0 = 2d_{(10)}/\sqrt{3}$.

Representative small angle XRD patterns are shown in Fig. 2A. Sample **Irr** shows the characteristic (10), (11) and (20) diffraction peaks of a 2-D hexagonal lattice (*p*6 mm). Samples **Sph$_{490}$**, **Sph$_{615}$** and **Sph$_{770}$**, typified by **Sph$_{615}$** in Fig. 2, also showed a distinctive (10) peak, but higher order peaks did not appear. This suggests a lowering of long-range order in the spherical MCM-41 particles. However, it should be pointed out that the small size of micro-spheres would also contribute to weaken high order diffraction peaks. The unit cell parameter a_0 deduced from the (10) reflection [35] was found to be approximately constant (within experimental error limit) for all **Sph** samples, independently of particle diameter, as shown in Table 1; for sample **Irr** a slightly larger value of a_0 was found. The small angle XRD patterns in Fig. 2A also show that the ordered mesoporous structure of MCM-41 is basically preserved after both, amine functionalization and ibuprofen loading. However, some broadening and shifting of the (10) diffraction peak is observed, as

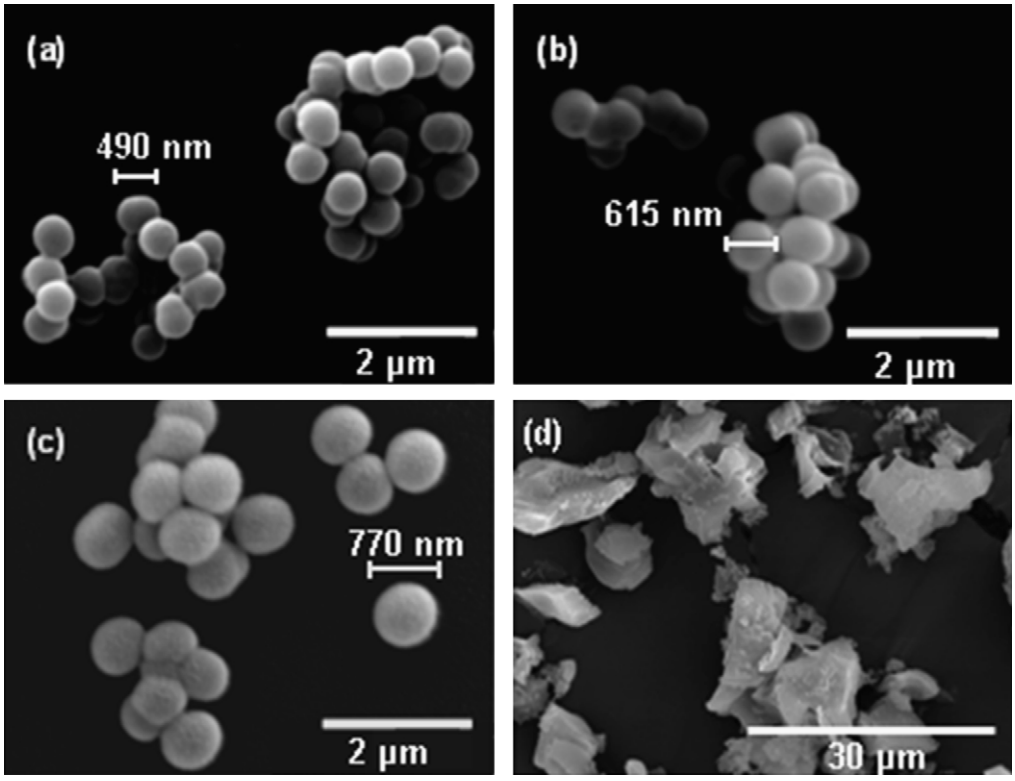

Fig. 1. Scanning electron micrographs of MCM-41 particles having spherical shape and different particle diameter: 490 nm (Sph490) (a), 615 nm (Sph615) (b) and 770 nm (Sph770) (c); and irregular particle morphology (d).

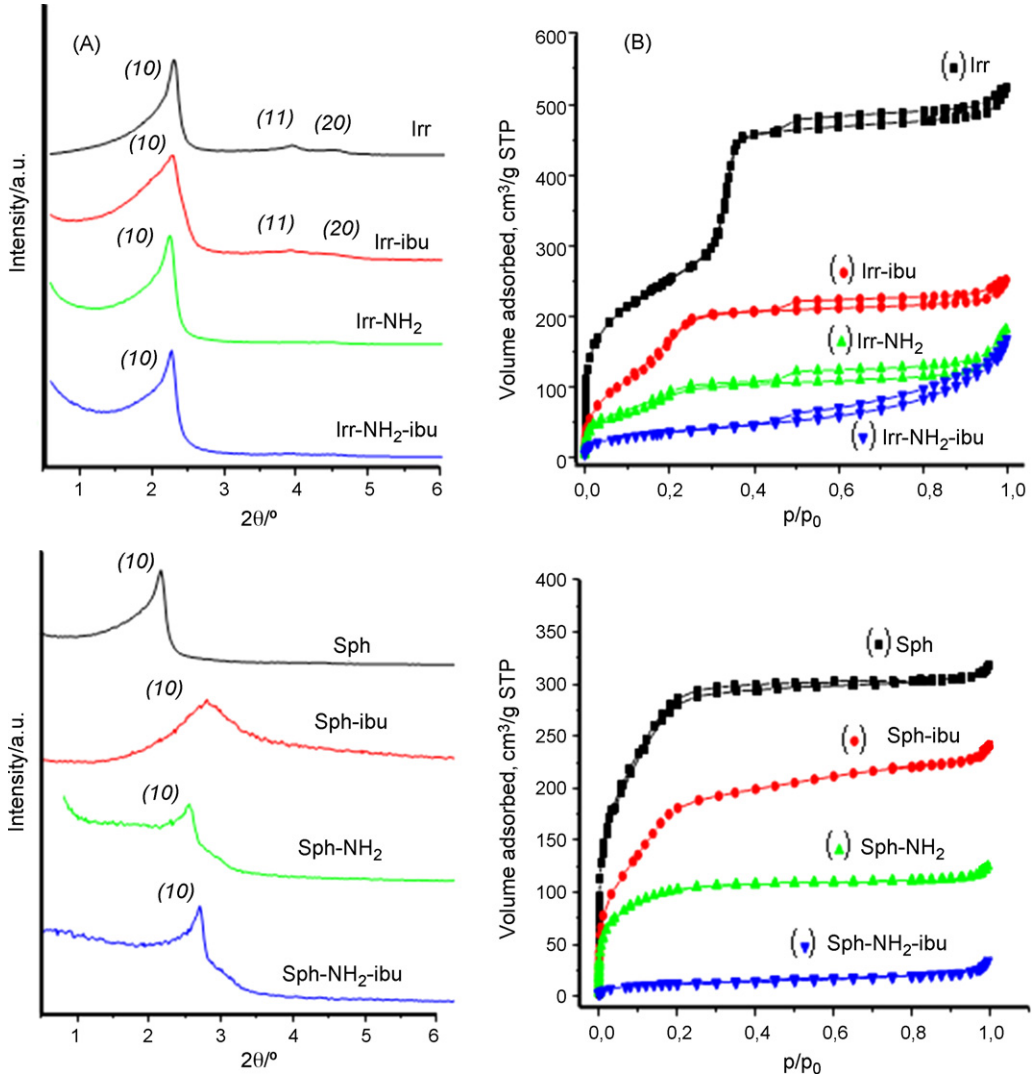

Fig. 2. (A) Small angle XRD patterns of MCM-41 consisting of irregularly shaped particles (Irr) and of MCM-41 nano-spheres (Sph). Amine-functionalized and ibuprofen-loaded samples are marked with $–NH_2$ and –ibu, respectively. (B) Nitrogen adsorption-desorption isotherms on the same samples.

well as a small variation of a_0 after functionalization (Table 2). Similar changes have been repeatedly reported in the literature [11,22,36,37] after both, functionalization and loading of mesoporous silicas with voluminous organic molecules. Detailed (rather complex) analysis of these small changes is outside the scope of this work, but it can be pointed out that several factors can contribute to the final result; among them partial hydrolysis of siloxane bridges during treatment procedures, mutual interaction between molecules of the organic phase and changes in overall background scattering of X-rays.

Table 2
Lattice parameter, a_0, and textural data for irregular and **Sph$_{615}$** samples before and after functionalization

Sample	a_0 (nm)	D_P (nm) KJS	V_P (cm3/g)	S_{BET} (m^2/g)
Irr	4.40	3.7	0.80	928
Irr-NH$_2$	4.53	2.8	0.23	341
Sph$_{615}$	4.11	3.1	0.48	1078
Sph$_{615}$-NH$_2$	4.02	2.1	0.18	356

The nitrogen adsorption–desorption isotherms (Fig. 2B) of both, unmodified and amine-modified samples can be considered as being type IV. For sample **Irr**, the nitrogen adsorption isotherm shows the typical step in the 0.1–0.3 relative pressure (p/p_0) range which is characteristic of a highly ordered mesoporous lattice [35,38]. **Sph** samples showed a less defined step, in consonance with the above commented results of X-ray diffraction. Sample **Irr** also shows clear sign of inter-particle porosity which gives rise to a hysteresis loop in the high relative pressure range, a feature that is often found [35,39] for similarly prepared MCM-41 materials. From the corresponding nitrogen sorption isotherms, specific (BET) surface area, pore diameter and total pore volume were calculated, using the KJS method [40] for textural analysis. Results for the pure silica MCM-41 samples are summarized in Table 1. After amine functionalization, a significant decrease in the total volume of adsorbed nitrogen (V_P) was observed (Fig. 2B and Table 2) for both, **Irr** and **Sph** samples. There is also a corresponding decrease of pore diameter (D_P) and specific surface area (Table 2). These observed facts testify the grafting of the organic moiety (aminopropyl group) to

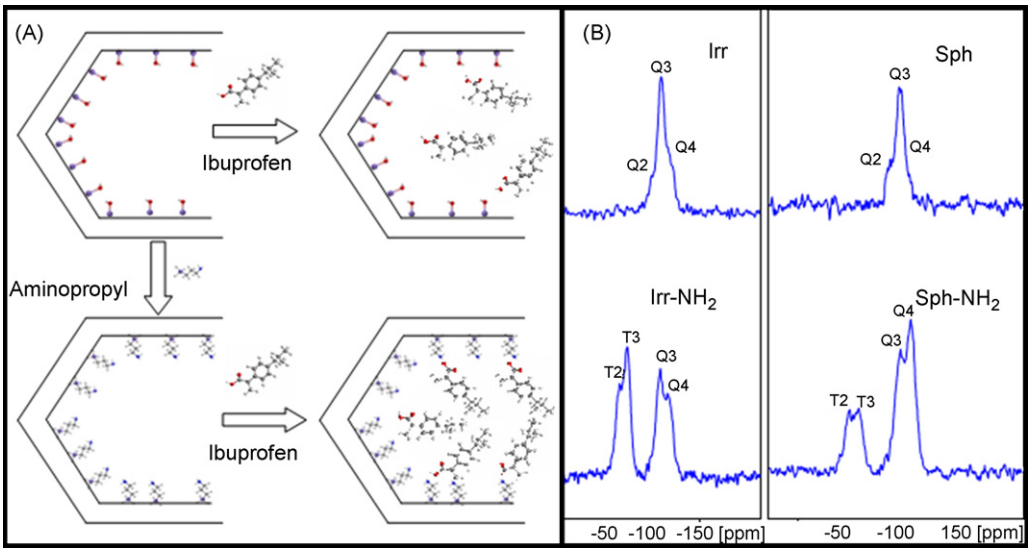

Fig. 3. (A) Scheme of aminopropyl grafting and ibuprofen loading into silica-based ordered mesoporous materials. (B) 29Si NMR spectra of Irr and Sph615 samples before and after aminopropyl grafting.

the internal pore wall, which leads (as expected) to less available space for adsorbed nitrogen. Similar behaviour was observed for other organic functionalized mesoporous silicas [19,21,22,41].

The organic functionalization of MCM-41 samples, both irregular and spherical, was also confirmed by ^{29}Si NMR measurements. Fig. 3B shows ^{29}Si-NMR spectra of unmodified and aminosilane modified MCM-41 materials. Before functionalization the most intense peak is Q^3 (at *ca.* −101.9 ppm) which suggests that the predominant silicon species are $(SiO)_3Si–OH$, as expected from a MCM-41 type material. As aminosilane grafting takes place, there is a marked increase on the Q^4 peak intensity (at *ca.* −108.9 ppm), which proves that there has been a conversion from $(SiO)_3Si–OH$ to fully condensed species due to grafting of aminopropyl group. This fact together with the presence of *T* species (T^3 at −68.5 ppm due to $RSi(OSi)_3$ species and T^2 at −59.7 ppm due to $(SiO)_2R'Si(OH)$ species) confirmed the grafting of the aminosilane reactant into the silica framework. Same trend was observed for both irregular and spherical MCM-41 particles (Fig. 3).

Organic functionalization was also evidenced by infrared spectroscopy which was carried out on all samples (spectra not shown). Typical ν(C-H) stretching vibrations of propyl chains at *ca.* 2900 cm^{-1}, together with $\delta(NH_2)$ bending bands at *ca.* 1570 cm^{-1} confirmed the grafting of amino propyl groups in all functionalized samples. As a visual aid, Fig. 3A shows a scheme of aminopropyl grafting and ibuprofen loading. A functionalization degree of 13% for all mesoporous samples was quantified using CHN elemental and thermogravimetric analyses.

Fig. 4 shows electron micrographs of MCM-41 spherical particles (sample **Sph$_{615}$**) before (a) and after functionalization (b), and also after ibuprofen loading (c). It is clearly seen that spherical shape is preserved throughout the whole process. However, particles show a trend to aggregate among themselves as a consequence of dispersion in pentane where silica is not soluble, and therefore the particles would aggregate to diminish the surface contact with the solvent.

3.2. Ibuprofen loading and release

Loading of ibuprofen into the host mesoporous materials was confirmed with FTIR analyses (not shown). The presence of carboxyl vibration bands at *ca.* 1720 cm^{-1}, together with C–H stretching vibrations in the 2950–2850 cm^{-1} range from the alkyl groups of ibuprofen, confirmed drug confinement into the host matrix. Fig. 2B shows that after drug loading a drastic decrease of pore volume and BET surface area occurred (as expected). This confirms that ibuprofen was adsorbed not only on external surfaces of the mesoporous materials, but mainly inside the pores, independently of the particle morphology. XRD patterns of ibuprofen loaded materials, Fig. 2A, show that the

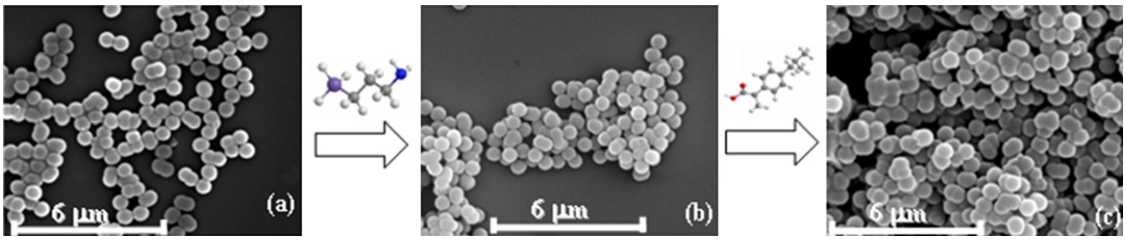

Fig. 4. Scanning electron micrographs of MCM-41 nano-spheres (sample Sph615) before (a) and after (b) aminopropyl grafting, and also after ibuprofen loading (c).

ordered mesoporous hexagonal framework was substantially maintained after the loading process.

Ibuprofen loading was quantified by using TG and elemental analyses. In all cases, irregular and spherical particles, approximately the same percentage of ibuprofen (*ca.* 25% by weight) was loaded into the purely siliceous mesoporous matrices. The amount of loaded ibuprofen was found to increase up to 30–36% in the amine-grafted materials, thus showing a considerable influence of functionalization on ibuprofen uptake. These results support a previous report [19] suggesting that functionalization is a major factor boosting drug uptake, while particle size and morphology show little effect. The protonated aminopropyl groups ($-NH_3^+$) anchored to the silica walls of MCM-41 act as attraction centres for carboxyl groups (–COOH) of ibuprofen molecules, and the resulting electrostatic interaction appears to be significantly stronger than hydrogen bonding (to silanols) in purely siliceous hosts.

The release profiles of ibuprofen from both functionalized and non-functionalized samples are shown in Fig. 5. As stated in Section 2.4 the *in vitro* tests were carried out by soaking ibuprofen loaded samples into a stirred SBF solution at 37 °C and pH 7.4. Under these conditions, ibuprofen release kinetics can be assumed to be controlled by diffusion along the ordered array of MCM-41 mesopores, since silica is nearly insoluble at pH 7.4. Delivery of ibuprofen to the SBF solution should therefore be determined by the Noyes-Whitney equation averaged over a small volume [42,43]:

$$\frac{dC_t}{dt} = k\bar{S}(C_S - C_t) \tag{1}$$

where C_t is the concentration of the solute at time t, S is the solvent accessible area per unit volume, C_S is the drug solubility in the equilibrium at the test temperature and k is a proportionality constant. It has been pointed out [44] that during drug release tests a small fraction of the drug might remain immobilized on the surface of the host solid; but this should not significantly affect results of kinetic measurements provided that such a small fraction remains approximately constant. Moreover, since the host matrix remains substantially unaltered during drug release tests, the diffusion coefficient (D) can be considered to be constant; and it should also be noted that C_t is only time dependent (since continuous stirring of the solution should avoid build-up of a concentration gradient). Under this approximation, the well-known [42] Fick's equations:

$$J = -D\frac{dC_t}{dx}, \quad \text{and} \quad \frac{dC_t}{dt} = D\frac{d^2C_t}{dx^2} \tag{2}$$

where J stands for the flux, allow the proportionality constant k of the Noyes-Whitney Eq. (1) to be related to the diffusion coefficient through Eq. (3) below:

$$k = \frac{1}{Vh}D \tag{3}$$

where V is the liquid dissolution volume of the molecules, that is taken as a constant in the present approximation and h is the width of the diffusion layer, *i.e.* the distance of the molecule from the point of adsorption to the outer solution. Rearranging constants and integrating Eqs. (1) and (2), the ibuprofen release can be represented by the following exponential decay equation:

$$\frac{w_t}{w_0} = 1 - e^{-k_1 t} \tag{4}$$

with w_t and w_0 being, respectively, the ibuprofen mass at time t and the initial mass of ibuprofen in the porous matrix. The release rate constant, k_1, is independent of ibuprofen concentration and contains information about the solvent accessibility and the diffusion coefficient through mesoporous channels. Taking these approximations into account, the release of ibuprofen depends on the amount of molecules adsorbed in the inner mesopore volume, being slower as the total mass of adsorbed ibuprofen diminishes. This model has previously been successfully applied for drug release from insoluble porous matrices having similar pore structure [19,45].

Experimental release profiles are shown in Fig. 5. It should be noted that in the test conditions release of ibuprofen from the mesoporous solid shows a slight deviation from the theoretical first-order behaviour described by Eq. (4). Drug delivery is faster in the initial testing time and achieves a stationary state after around 48 h, for pure silica samples and 150 h for functionalized MCM-41. The observed divergence from the theoretical model can be attributed (mainly) to the fact that desorption of a drug molecule from a mesopore wall is affected by steric hindrance exerted not only by grafted functional groups (in functionalized

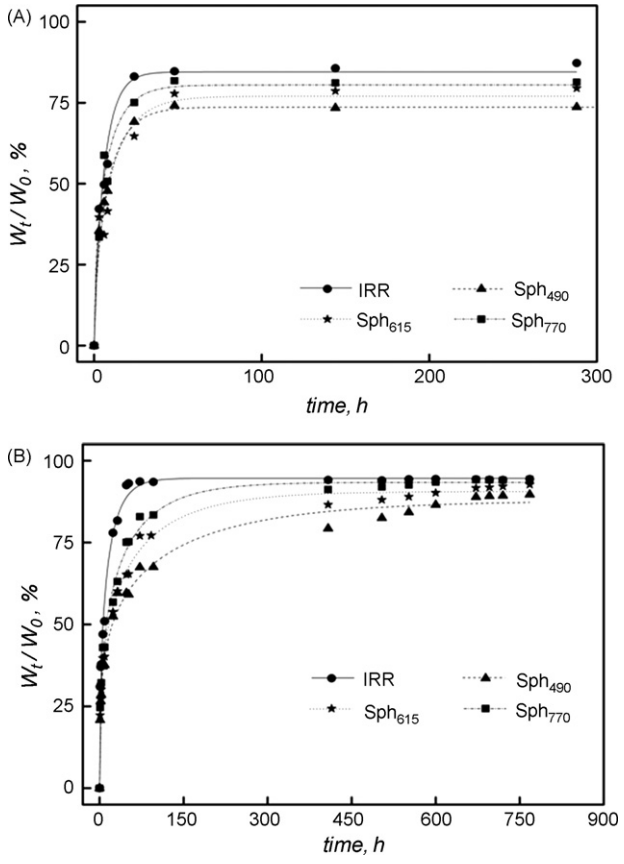

Fig. 5. Release profiles of ibuprofen from purely siliceous (A) and amine-functionalized (B) MCM-41 samples. (Note the different time scale).

Table 3
Kinetic parameters of ibuprofen release from MCM-41 samples

Sample	w_0 (mg/g)	$(w_t/w_0)_{max}$ (%)	$k_1 \times 10^3$ (h^{-1})	δ	χ^2
IRR	260 ± 5	85 ± 3	145 ± 12	0.90 ± 0.09	20.9
Sph_{490}	260 ± 6	74 ± 2	89 ± 4	0.18 ± 0.03	5.74
Sph_{615}	250 ± 7	77 ± 4	71 ± 6	0.31 ± 0.02	44.6
Sph_{770}	250 ± 4	80 ± 3	90 ± 9	0.50 ± 0.19	25.6
IRR-NH_2	360 ± 6	94 ± 1	41 ± 6	0.42 ± 0.04	8.60
Sph_{490}-NH_2	310 ± 7	88 ± 2	5 ± 1	0.25 ± 0.02	7.35
Sph_{615}-NH_2	330 ± 5	91 ± 1	9 ± 1	0.30 ± 0.02	3.91
Sph_{770}-NH_2	300 ± 7	93 ± 1	12 ± 1	0.32 ± 0.02	4.47

w_0: initial loaded mass (mg Ibu/g SiO_2); $(w_t/w_0)_{max}$: maximum relative release; k_1: release rate constant; δ: kinetic non-ideality factor; χ^2: goodness of fit.

samples) but also by the remaining drug molecules. Deviation from the theoretical first-order kinetic model was accounted for by introducing an empirical non-ideality factor (δ) in Eq. (4) to yield:

$$\frac{w_t}{w_0} = (1 - e^{-k_1 t})^{\delta} \quad (5)$$

Values for δ are comprised between 1, for materials that follow first-order kinetics, and 0 for materials that release the loaded drug in the very initial time of analysis; due to rapid delivery of drug molecules located only at pore entrances.

Taking into account the above considerations, the drug release profiles of both **Irr** and **Sph** samples, before and after functionalization, were fitted using the non-ideal first-order kinetic model and the obtained values of release parameters are shown in Table 3, together with the goodness of fit to Eq. (5) expressed as χ^2. Lower values of χ^2 point to a more accurate approximation to the proposed model, and they are usually smaller than 20. The final amount of ibuprofen released from each sample is not too far from the total loaded amount (Fig. 5 and Table 3) and, most important, functionalization does not result in final retention of a higher percentage of the drug. However, functionalized samples do show a significantly slower release rate, as seen in Fig. 5. Note that the plateau corresponding to maximum delivery is reached after about 50 h for non-functionalized samples (Fig. 5A) while a considerably larger time is needed for functionalized hosts (Fig. 5B). Quantitatively, this can more conveniently be referred to the corresponding values of the kinetic k_1 parameter (Table 3). When comparing the **Irr** with **Sph** samples, it becomes clear that the host matrix consisting of irregular MCM-41 particles shows faster drug delivery kinetics. The greater pore size of irregular samples compared to spherical ones could also contribute to the different delivery rates observed. In addition, different diffusion paths for ibuprofen within materials with different morphology could also promote different release rates. This is so much the case when considering functionalized materials, for which the kinetic k_1 parameter strongly decreases (well over 70%) when going from **Irr-NH_2** to the **Sph-NH_2** samples. Among the latter, drug delivery rate shows a tendency to decrease the smaller the micro-sphere size. In addition, as above mentioned for unmodified samples, we cannot discard the effect of pore size in release kinetics. However, the short range of sizes tested precludes conclusive analysis of this factor.

In essence, what this study clearly shows is that ibuprofen delivery can best be controlled by using amine-functionalized MCM-41 mesoporous silica in the form of monodispersed and microsized silica spheres. Irregularly shaped (and heterogeneously sized) MCM-41 powders provide significantly less control. This work confirms this type of materials as model systems for drug delivery technologies and opens the gates to new incoming ideas in this field. As a possibility, these microsized spheres could be uniform coated with a protective thin layer of an organic polymer. A convenient choice of such a polymer would enable targeting of drug delivery. For instance, a polymer that would hydrolyze at a pH higher than 6 but not at pH 1–3 should facilitate oral administration of stomach degradable drugs (*e.g.* those which are protein based) which could be safely targeted to the intestinal track.

4. Conclusions

Ibuprofen loading into mesoporous MCM-41 silica and subsequent drug release to a simulated body fluid was analyzed for both, irregularly shaped MCM-41 samples and monodispersed microsized spheres. The effect of amine functionalization was also investigated. Main conclusions are as follows.

(I) For non-functionalized MCM-41 materials, drug release rate shows little dependence on carrier morphology, and, therefore, from an industrial point of view, it is worthless to expend time, money and effort designing a determined particle morphology. The easiest and cheapest industrial procedure should be employed.

(II) Amine-functionalization of MCM-41 leads to a significant increase (by about 10%) on loading capacity of the mesoporous drug host, regardless of particle shape and size. However, slight differences in the drug release profiles were found for modified materials. In this case the mesoporous carrier prepared in the form of microsized spheres showed a distinctively slower drug release rate than that consisting of irregularly shaped (and sized) powders. Among spherical particles, those having smaller size tend to show slower drug release kinetics. Therefore, microsized (functionalized) MCM-41 spheres seem to be superior to irregularly shaped MCM-41 powders as carriers for controlled drug release formulations.

References

[1] A. Rutkowska, W. Piekozewski, J. Brandys, Biopharm. Drug Dispos. 20 (1999) 117.
[2] M.H. Smolensky, E. Haus, Am. J. Hypertens. 14 (2001) 280.
[3] A. Dashevsky, A. Mohamad, Int. J. Pharm. 318 (2006) 124.
[4] P. Horcajada, A. Rámila, J. Pérez-Pariente, M. Vallet-Regí, Microporous Mesoporous Mater. 68 (2004) 105.
[5] S. Sant, V. Nadeau, P. Hildgen, J. Control. Release 107 (2005) 203.
[6] M. Vallet-Regí, Chem. Eur. J. 12 (2006) 5934.
[7] M. Stempniewicz, M. Rohwerder, F. Marlow, Chem. Phys. Chem. 8 (2007) 188.
[8] M. Vallet-Regí, F. Balas, D. Arcos, Angew. Chem. Int. Ed., in press.
[9] M. Vallet-Regí, F. Balas, M. Colilla, M. Manzano, Solid State Sci. (2007), doi:10.1016/j.solidstatesci.2007.03.026.
[10] B.G. Trewyn, C.M. Whitman, V.S.Y. Lin, Nano Lett. 4 (2004) 2139.
[11] P. Horcajada, A. Rámila, G. Férey, M. Vallet-Regí, Solid State Sci. 8 (2006) 1243.
[12] Y. Ito, H. Arai, K. Uchino, K. Iwasaki, N. Shibata, K. Takada, Int. J. Pharm. 289 (2005) 69.
[13] A. Sayari, Y. Yang, M. Kruk, M. Jaroniec, J. Phys. Chem. B 103 (1999) 3651.
[14] S. Liu, L. Lu, Z. Yang, P. Cool, E.F. Vansant, Mater. Chem. Phys. 97 (2006) 203.
[15] A. Zukal, M. Thommes, J. Cejka, Microporous Mesoporous Mater. 104 (2007) 52.
[16] M. Vallet-Regí, A. Rámila, R.P. del Real, J. Pérez-Pariente, Chem. Mater. 13 (2001) 308.
[17] C.Y. Lai, B.G. Trewyn, D.M. Jeftinija, K. Jeftinija, S. Shu, S. Jeftinija, V.S.Y. Lin, J. Am. Chem. Soc. 125 (2003) 4451.
[18] I.I. Slowing, B.G. Trewyn, S. Giri, V.S.Y. Lin, Adv. Funct. Mater. 17 (2007) 1225.
[19] F. Balas, M. Manzano, P. Horcajada, M. Vallet-Regí, J. Am. Chem. Soc. 128 (2006) 8116.
[20] D.R. Radu, C.Y. Lai, K. Jeftinija, E.W. Rowe, S. Jeftinija, V.S.Y. Lin, J. Am. Chem. Soc. 126 (2004) 13216.
[21] B. Muñoz, A. Rámila, J. Pérez-Pariente, I. Díaz, M. Vallet-Regí, Chem. Mater. 15 (2003) 500.
[22] A. Rámila, B. Muñoz, J. Pérez-Pariente, M. Vallet-Regí, J. Sol-Gel Sci. Technol. 26 (2003) 1199.
[23] P. Horcajada, C. Serre, M. Vallet-Regí, M. Sebban, F. Taulelle, G. Férey, Angew. Chem. Int. Ed. 45 (2006) 5974.
[24] C.T. Kresge, M.E. Leonowicz, W.J. Roth, J.C. Vartuli, J.S. Beck, Nature 359 (1992) 710.
[25] J.S. Beck, J.C. Vartuli, W.J. Roth, M.E. Leonowicz, C.T. Kresge, K.D. Schmitt, C.T.-W. Chu, D.H. Olson, E.W. Sheppard, S.B. McCullen, J.B. Higgins, J.L. Schlenker, J. Am. Chem. Soc. 114 (1992) 10834.
[26] M. Grün, I. Lauer, K.K. Unger, Adv. Mater. 9 (1997) 254.
[27] W. Stöber, A. Fink, E. Bohn, J. Colloid Interface Sci. 26 (1968) 62.
[28] R.I. Nooney, D. Thirunavukkarasu, Y. Chen, R. Josephs, A.E. Ostafin, Chem. Mater. 14 (2002) 4271.
[29] Y. Zhu, J. Shi, W. Shen, H. Chen, X. Dong, M. Ruan, Nanotechnology 16 (2005) 2633.
[30] Y. Zhu, J. Shi, Y. Li, H. Chen, W. Shen, X. Dong, Microporous Mesoporous Mater. 85 (2005) 75.
[31] B. Onida, V. Cauda, S. Fiorilli, E. Garrone, E. Vernè, C. Vitale Brovarone, P. Appendino, D. Viterbo, G. Croce, Stud. Surf. Sci. Catal. 158B (2005) 2027.
[32] C. Armstrong, Arch. Clin. Neuropsychol. 10 (1995) 1.
[33] J.G.M. van Engelen, W. Rebel-de Haan, J.J.G. Opdam, G.J. Mulder, Toxicol. Appl. Pharmacol. 144 (1997) 385.
[34] T. Kokubo, H. Kushatani, S. Sakka, T. Kitsugi, T. Yamamuro, J. Biomed. Mater. Res. 24 (1990) 721.
[35] M. Kruk, M. Jaroniec, A. Sayari, Chem. Mater. 11 (1999) 492.
[36] B. Onida, B. Bonelli, L. Flora, F. Geobaldo, C. Otero Areán, E. Garrone, Chem. Commun. (2001) 2216.
[37] S.W. Song, K. Hidajat, S. Kawi, Langmuir 21 (2005) 9568.
[38] M. Kruk, M. Jaroniec, J.M. Kim, R. Ryoo, Langmuir 15 (1999) 5279.
[39] G. Turnes Palomino, J.J. Cuart Pascual, M. Rodríguez Delgado, J.B. Parra, C. Otero Areán, Mater. Chem. Phys. 85 (2004) 145.
[40] M. Kruk, M. Jaroniec, A. Sayari, J. Phys. Chem. B 101 (1997) 583.
[41] A.S.M. Chong, X.S. Zhao, J. Phys. Chem. B 107 (2003) 12650.
[42] J. Crank, The Mathematics of Diffusion, second ed., Oxford University Press, Oxford, 1975.
[43] P. Costa, J.M. Sousa-Lobo, Eur. J. Pharm. Sci. 13 (2001) 123.
[44] G. Frenning, M. Strømme, Int. J. Pharm. 250 (2003) 137.
[45] N.V. Mulye, S.J. Turco, Drug Dev. Ind. Pharm. 21 (1995) 943.